RSC Advances

ROYAL SOCIETY OF CHEMISTRY

www.rsc.org/advances

The table of contents:

MWCNT/PAN aerogel composites were synthesized using the Thermal Induced Phase Separation (TIPS) procedure.

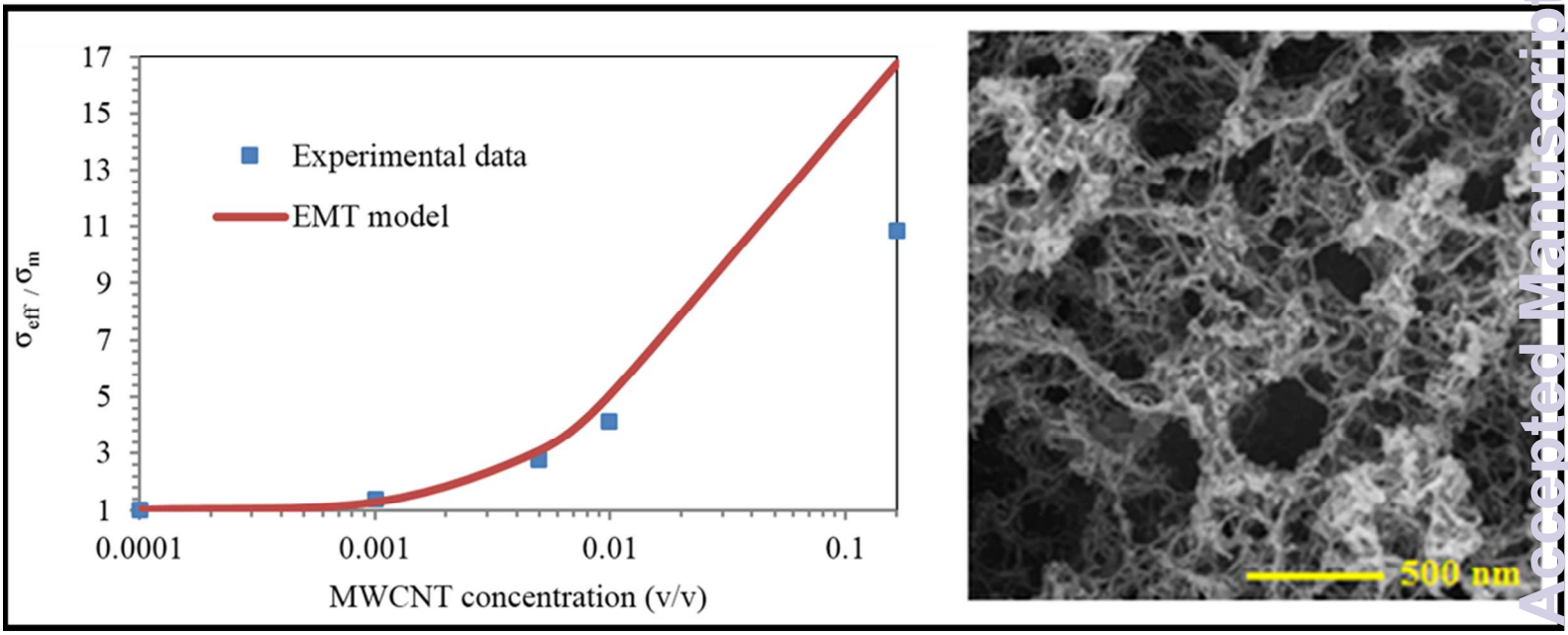

Journal Name

ARTICLE

Morphology and electrical properties of multi-walled carbon nanotube/carbon aerogel prepared by using Polyacrylonitrile as precursor

Received 00th January 20xx,
Accepted 00th January 20xx

DOI: 10.1039/x0xx00000x

www.rsc.org/

A. Dourani, [a, b] M. Hamadanian, *[b] M. Haghgoo *[a], M. R. Jahannama [a] and H.Goudarzi [a]

Here, we present the synthesis and characterization of low-density Multi-walled carbon nanotube (MWCNT) /carbon (CA) aerogel by creating a three-dimensional assembly of carbon nanotubes (CNTs) in Polyacrylonitrile (PAN)/Dimethyl formamide(DMF) solution to create a stable gel, followed by a CO_2 supercritical drying. Aerogels with varying nanotube loading (0–25 wt. %) and density (50–500mg cm^{-3}) were fabricated and characterized by optical microscopy, electron microscopy, nitrogen sorption and electrical conductivity analysis. Physical properties of the MWNT/CA composites were highly dependent upon nanotube loading. The data indicate that the shrinkage value decreases gradually during drying and pyrolysis process when MWCNT content increases in formulations. Surface area as high as 735 m^2/g was achieved for MWNT/PAN aerogel with carbon nanotube loading higher than 20 wt. % .

Introduction

Aerogels are highly porous materials with the lowest density of any other solid substance. [1-3] They are usually meso-to macroporous with little microporosity.[4] Aerogels have attracted the attention of researchers for faster response to sensing, energy storage, and energy conversion than other pore-solid architectures.[5] Their unique microstructure originates from their wet chemical preparation by the solution sol-gel method [6] or phase separation techniques [7] and their subsequent liberation from the solvent via supercritical drying. Thermally induced phase separation (TIPS) is currently utilized to fabricate microporous membranes or microcellular foams. This technique is based on the principle that a single homogeneous solution of polymer/solvent or polymer/solvent/non-solvent at elevated temperature is converted via the removal of thermal energy to two-phase separated domains composed of a polymer-rich phase and a polymer-lean phase. According to whether the quenching end point is located in the metastable region between binodal and spinodal curves or in the unstable region below the spinodal curve, two distinguished morphologies can be obtained: (i) a poorly interconnected bead-like structure by a nucleation and growth mechanism or (ii) a well-interconnected open porous structure by a spinodal decomposition mechanism. It is necessary to preferably utilize the spinodal decomposition for the production of open-pore microcellular foams. Pore size distribution and their interconnectivity of the resultant microcellular foams are determined by an exact balance of various parameters such as polymer concentration, quenching route, quenching depth, solvent/non solvent composition, and the presence of additives.[8-10] Carbon nanotubes (CNTs) have distinctive particular, such as high aspect ratio, small diameter, light weight, high mechanical strength, high electrical and thermal conductivities and unique optical and optoelectronic properties .[11,12] By combining extraordinary properties of CNTs with those of aerogels, a new class of materials becomes accessible with unique multifunctional material properties, which may find applications in energy storage devices, advanced catalyst supports, energy absorption materials, multifunctional composites, chemical and biological sensors,etc.[13-15] Islam [16-20] and coworkers created the polyvinyl alcohol reinforced CNT aerogels from wet CNT-surfactant gel precursors, and they showed that the composites (with typical CNT loadings ranged from 25 to 33 wt. %) are strong and electrically conductive (10^{-2} S/cm). They showed that these aerogels have open-cell structures and their Young's moduli are higher than other aerogels at comparable density. The organic functionalization of either single-walled carbon nanotube (SWCNTs) or multi-walled carbon nanotube (MWCNTs) with a crosslinker can result in the formation of freestanding CNT aerogels. For instance, Chen [21,22] and coworkers showed that SWNTs functionalized by ferrocene grafted poly (p-phenyleneethynylene) can gelate common organic solvents such as chloroform to form a robust 3D nanotube networks that cannot be re-dispersed in any organic solvent within the context of monomers and polymers. Zhang et al. [23,24] demonstrated that embedding either MWCNTs or acid-treated MWNTs in to a poly(3,4-ethylenedioxythiophene)–poly(styrenesulfonate)(PEDOT–PSS) aerogel matrix can significantly enhance the specific surface areas (280–400 m^2/gr) of the resulting composite aerogels while maintaining good thermal stability and electrical conductivity (1.2–6.9×10^{-2} S/cm). In another study Zhai [25]and coworkers used poly (3-(trimethoxysilyl) propylmethacrylate) (PTMSPMA) to disperse and functionalize MWCNTs. They reported that strong and permanent chemical bonding between percolated MWCNTs in the resulting free-standing monolithic aerogel was obtained upon the hydrolysis

[a] Space transportation research institute, Iranian research Center, Department of Nanotechnology & Nanoscience, Tehran, I.R.Iran. E-mail: majid.haghgoo@gmail.com
[b] Institute of Nano Science and Nano Technology, University of Kashan, Kashan, I. R. Iran, E-mail: hamadani@kashanu.ac.ir
DOI: 10.1039/x0xx00000x

and condensation of PTMSPMA. The entangled MWCNTs generated mesoporous structures on the honeycomb walls; creating aerogels with a surface area of 580 m^2/g, remarkable elastic properties and good electrical conductivity (e.g. up to 0.67 S/cm). All these features determined the exceptional pressure and chemical vapor sensing capabilities of MWCNT/ PTMSPMA aerogels. Worsley [26-30] and coworkers have performed a quite extensive and stimulating work on SWCNT and DWCNT three-dimentional architectures synthesized by resorcinol–formaldehyde (RF) polycondensation. After introduction of precursors to a suspension of highly purified SWCNTs, the polymerization was primarily induced on the walls of the CNT bundles and, more importantly, at the junctions between adjacent bundles to form a CNT/RF wet gel. The resulting assembly was dried and subsequently pyrolyzed to convert the organic part into carbon. The resultant SWCNT/CA were mechanically robust and highly electrically conductive (up to 1.12 S/cm) showing specific surface area up to 184 m^2/g, which are excellent materials for multifunctional composites. Haghgoo et al. [31, 32] studied the effect of dispersion state of nanotubes on physical properties of RF aerogel. Their results showed that the MWCNTs were completely exfoliated in the MWCNT /RF composite throughout RF aerogel at low nanotube content (<0.26 v %), whereas at higher concentrations, MWCNTs came into contact with each other to form aggregates. They demonstrated that the MWCNT depletion attraction in the presence of NaDBS in the reaction mixture might account for this effect. The presence of MWCNT aggregates affected the porous properties of aerogels by reducing the effective micropore volume and also led to a deviation of the thermal conductivities of the nanocomposites from the expected values calculated by effective medium theory (EMT). In this article we report a new approach to the synthesis of stable CNT aerogels. Thermally induced phase separation (TIPS) method was used for preparation of a freestanding MWCNT/polyacrylonitrle (PAN) aerogels monolith. A review of the literature shows TIPS method has not been used to prepare CNT aerogels. PAN is a very suitable precursor to prepare carbon aerogels with excellent performance because of its high melting point, considerable carbon yield, and relatively cheap price. It is accepted [33] that fast pyrolysis of PAN generates a graphitic structure by thermal stabilization and subsequent carbonization. The good dissolution of PAN and proper dispersion of functionalized CNTs in the polar solvent N,N-dimethylformamide, allows a better control of the final composition of the two phases. This report also describes the influence of MWNT loading as well as the synthesis conditions of the polyacrylonitrile binder on the microstructure and electrical conductivity of the MWNT/CA composites.

2. Experimental

2. 1. Materials

Polyacrylonitrile (PAN) powder (with the molecular weight of approximately 150,000 g/mol) was purchased from Aldrich Chemical Co. DMF (N, N-dimethyl formamide) and acetone were obtained from Merck. The COOH Functionalized Multi walled Carbon Nanotubes (COOH-MWCNTs) (purity> 95%, COOH content ~2.56 wt. %) were purchased from PlasmaChem (Germany). Their length, outer diameter and number of walls were 5.8 µm, 8–15 nm and 3–12, respectively. Deionized water was used in all cases.

2.2. Synthesis of pure and composite aerogels

At the first stage, a homogeneous solution of PAN (typically 4 wt. %) was prepared by adding 1.17 grams of PAN to 25.15 cc of DMF. Subsequently, 4.10 cc of water was slowly added to the solution at 150 ˚C to make a mixture of DMF / water (84:16 v/v). In this composition, separation region is narrow for the ternary system of PAN/DMF/water and the probably of liquid-liquid phase separation is stronger. Therefore, the forming of a cellular structure is more probable[14,34].

When the solution was clear and homogenous, it was poured in to a warm cylindrical mold and quenched to room temperature with a cooling rate of 10˚ C/min to obtain a polymer gel. Then, DMF was exchanged with acetone over 32hr (fresh acetone was added every 8hr). Finally, the wet gel was dried supercritically (above CO_2 critical pressure and temperature, 32 ˚C and 72 bar, respectively) to create polyacrylonitrile aerogel. The PAN aerogel (8 wt. %) was prepared exactly as described above; The only difference was that the PAN concentration became doubled. The dry PAN aerogel was pretreated in a forced-air convection oven at 220˚C for 12 hr, followed by pyrolysis at 850 ˚C under an argon atmosphere for 6 hr at a rate of 5˚C/min.

For composite aerogels, COOH-MWCNTs were dispersed in DMF by sonication at 80 W and 24 kHz in 30 min. Then the PAN powder was added to the resulting suspension and the whole mixture was further ultrasonicated for 30 min. Afterwards, the solution was stirred and heated up to 150˚C, and appropriate amount of deionized water , (DMF/water equal to 84/16 v/v) was added drop by drop to the mix. The concentration of MWCNTs in the reaction mixture ranged from 0 to 25 wt. %. Other steps include solvent exchange, drying and pyrolysis was done similar to these applied to carbon aerogel. In the next sections, the samples are denoted as follows: 'PA' and 'CNT' stands for polyacrylonitrile and carbon nanotube aerogel respectively. 'PA ' is followed by the weight percentage of PAN in the primary mixture and 'CNT' is followed by the concentration of carbon nanotube in the final composite. In the nomenclature, 'PA' is change to 'CA' after pyrolysis of the sample.

2.3. Physical characterization

The bulk density, ρ_b, of the aerogels was calculated from the dimensions and weight of monolithic cylindrical samples and the skeletal density, ρ_s , was obtained from the raw material brochure. The skeletal density of the hybrid aerogel was calculated using the rule of mixtures. Indeed, from bulk and skeletal densities, it is made possible to calculate the porosity percent ($\mathcal{E}$) and pore volume (V_{total}) of the gels as follows: [35]

$$\boldsymbol{V}_{\mathbf{total}} = \frac{\mathbf{1}}{\boldsymbol{\rho}_b} - \frac{\mathbf{1}}{\boldsymbol{\rho}_s} \quad (1)$$

$$\mathcal{E} = \left(\mathbf{1} - \frac{\boldsymbol{\rho}_b}{\boldsymbol{\rho}_s}\right) \times 100 \quad (2)$$

The linear shrinkage of the gels was calculated simply by comparing the diameter of the samples before and after drying and was reported as radial shrinkage percent. Internal surface area determination and pore size analysis were performed by the Brunauer–Emmett–Teller (BET) and Barrett–Joyner–Halenda methods using a Sorptomatic 1990 apparatus respectively. Samples of approximately 0.1 g were heated to 120 ˚C under vacuum (10^{-5} Torr) for at least 24h to remove all adsorbed species. In order to obtain information regarding pores larger than 50 nm, which cannot be investigated by nitrogen adsorption, mercury

porosimetry was performed with a Thermofinnigan Pascal 140. The analysis was carried out porosimeter between 0.01 and 200 MPa after outgassing the sample for 2h at room temperature and under vacuum. The dispersion state of MWCNTs throughout the composites was analyzed by optical microscopy using an Olympus PROVISAX70 microscope. The samples were prepared by embedding a piece of the material in epoxy resin and cutting a slice by a steel knife. The morphology of the samples were observed by scanning electron microscopy (Field Emission-SEM) using a TESCAN LYRA3 apparatus. Before observation, samples were first fractured in liquid nitrogen and sputter coated with Au/Pd. Transmission electron microscopy (TEM) was used to investigate the dispersion state of the CNTs. TEM imaging was performed using a Carl Zeiss(LIBRA 200 MC ,Carl Zeiss SMT, Germany) transmission electron microscope (operated at 200 kV). As for preparation, MWNT was ultrasonically dispersed in DMF for 1 hr and then diluted to 1:60 and dropped on a TEM grid. TGA was performed using Perkin–Elmer TGA7 thermogravimetric analyzer from room temperature to 1000 °C at 10 °C/min in N_2 atmosphere. The weight of samples was 8±2 mg in all cases. Electrical properties were measured using two-probe measurements (EC-Lab V10 and Fluke Ohmmeter). Metal electrodes were attached to the ends of the cylindrical samples (0.5 cm thick and 1 cm diameter) with silver paste.

Results and discussion

Fig. 1 presents the macroscopic morphology of nanotube dispersion in the aerogel. A homogeneous distribution of nanotubes clusters can be observed. Only a few micro clusters of MWCNTs were observed as isolated dark particles, but these can be neglected without loss of accuracy. In the case of higher MWCNT concentration in composites (e.g. sample Fig. 1b), the number and

the size of MWCNT clusters became higher and dark areas with size of several micrometres was observed. Some clusters were connected to each other and a continuous CNT phase within the polymer matrix was created.

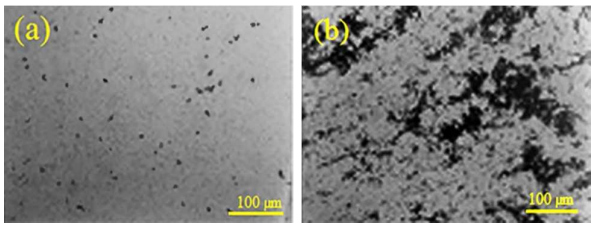

Fig. 1. Optical micrographs of (a) 0.01 v/v % MWNT/PAN aerogel (b) 16.5 v/v % MWNT/PAN

Fig. 2 shows the cross-section and surface morphologies of PAN aerogel prepared from the ternary system (PAN, DMF, water) with different PAN contents. All the aerogels showed symmetric morphology full of cellular pores. The aerogel fabricated from 4 wt. % PAN exhibited honeycomb-like morphology with large pores. As the PAN concentration increased to 8 wt. %, channel-like structure appeared and 3D fibrous structure of interconnected PAN aerogel was observed (Figs. 2c).

It must be mentioned that the pore structure of PAN aerogel is significantly controlled by the polymer concentration and strongly dependent on the droplet growth. The honeycomb-like pores originate from the isotropic morphology, whereas the channel-like pores result from the anisotropic morphology of droplets. In the case of a mixture with low PAN concentration, the diluent molecules easily aggregate into large crystals; as for the mixture containing higher PAN amount, the diluent molecules would be fixed at an adjacent nucleus prior agglomeration [9].

SEM images showed that the pore size reduces with increasing of PAN concentration in the ternary system. Similar results have been reported by Xu et al [8-10] in polar polymer membranes. Their results indicated that the pore size was decreased from 5.3 to 0.8 µm with the increasing of PAN concentration from 10 wt. % to 22 wt. % . They attributed that to the increasing viscosity of the PAN/DMF solution, which prevents the crystallization of PAN , resulting in smallness of pores.

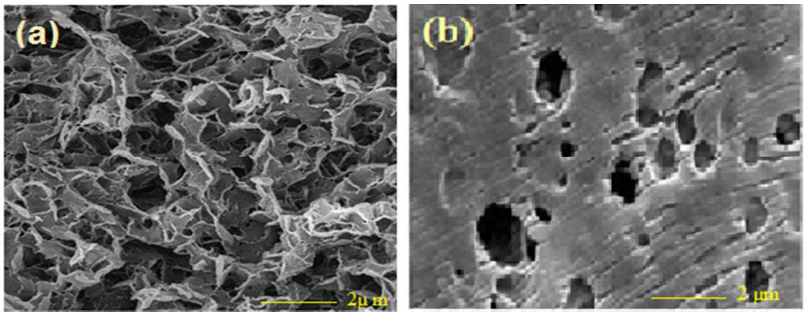

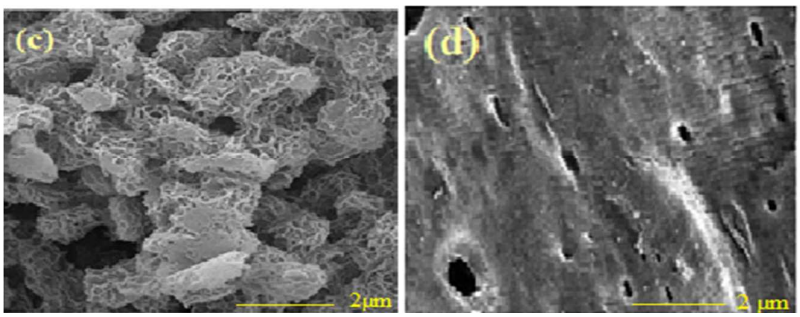

Fig. 2. SEM images of PAN aerogel prepared from 4wt. % PAN: cross-section (a) , top surface (b) and 8 wt. % PAN: cross-section (c), top surface (d) with different magnification

The microstructure of the MWNT/PAN aerogels with CNT loadings ranging from 0.01 to 1 v/v% were evaluated using scanning electron microscopy (SEM) in Fig. 3. The structural analysis of the aerogels revealed a highly porous interconnected network consisting of randomly oriented CNTs, with pore sizes ranging from tens of nanometres up to several micrometres.

In general, from the SEM images, MWCNTs were found to be fairly uniformly dispersed and distributed across the PAN matrix, increasing the probability of forming an interconnected carbon nanotube network.

It was also observed that PAN was concentrated at the CNT joints and connected within the CNT assembly. With increasing concentrations of nanotubes, the wide network of filament-like structures was formed within the aerogels and it seems that more MWCNTs are located at the surface of the PAN matrix and also they connect the pores following channel-like architecture.

Similar results have been reported by Zhang et al. [36], in preparation of CNT assembly by infiltration PAN in to CNT sheet and yarns by the dip –coating method. Their report illustrated that PAN was concentrated at the CNT joints and changed in to graphitic structure after carbonization treatment .

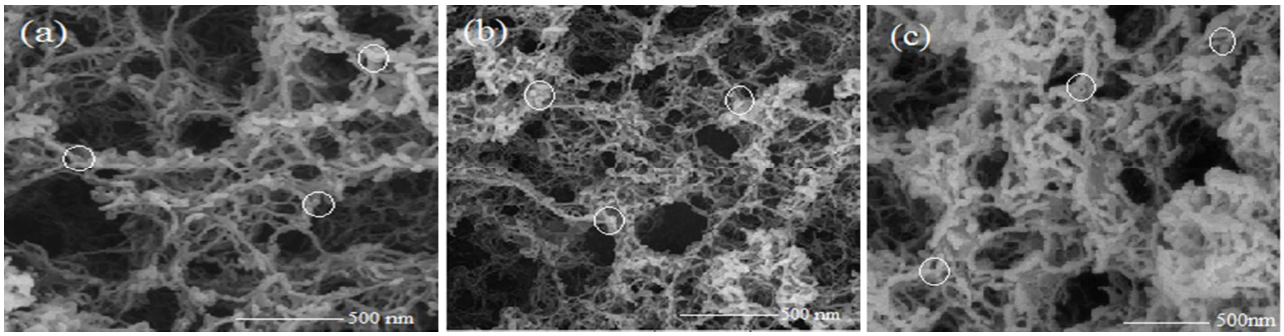

Fig.3. SEM images of (a) PA4-CNT0.01 (b) PA4-CNT0. 1 and (c) PA4-CNT1. White circles show aggregation of PAN at the nodes between nanotubes

TEM micrograph of a typical carbon nanotube suspension (0.01 v/v% after 60 min sonication) is shown in Fig. 4 with different magnifications. The images showed that the most of MWCNTs were isolated and disentangled. From Fig. 4a, could be estimated that the length of the tubes, decreased by about 1 µm and from Fig. 4b , could be estimated that the diameters of MWCNTs were typically in the range of 8 to 15 nm. Therefore, it can be concluded that the fragmentation of carbon nanotubes induced by sonication and experiments showed that CNT length drops with sonication time but the diameter of the nanotubes are not changed during sonication. Histogram of the CNT diameters (Fig. 4c) demonstrate relatively narrow distributions with average diameters of 15.14 nm.

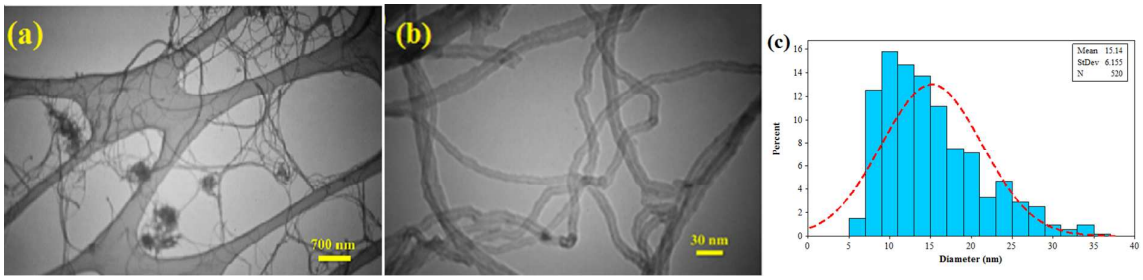

Fig. 4. Typical TEM images of MWCNT suspension with (a) low and (b) high magnification . Corresponding histogram of the nanotube diameter was plotted in Fig 4. (c) . The dash lines correspond to Gaussian fit.

The bulk density of the samples ranged from 0.05 to 0.82 g/cm^3. The skeletal density of PAN, pyrolyzed PAN [9] and MWCNT were found to be 1.18, 1.75 and 2.1 g/cm^3 respectively.

Fig.5 shows typical adsorption–desorption isotherm and mercury porosimetery curve of the samples; here, P is the equilibrium pressure and P_0 is the saturation pressure of the adsorbents at the adsorption temperature of 77 K. The MWCNT/PAN and MWCNT/CA aerogels both exhibit a hybrid of type II and type IV isotherms (Fig. 5a). Fig.5b shows the mercury porosimetry curves obtained for the MWCNT/PAN and MWCNT/CA aerogels. The results showed that the pore size distribution of the aerogel samples was very broad from the mesoporous to the macro porous regime. The pore sizes of the carbon aerogel are smaller than that of the PAN aerogel, indicative of the shrinkage of the whole sample during the carbonization process. A comparison of the MWCNT/PAN aerogels in terms of macroporosity revealed that the pore size of the aerogels decreased gradually with increasing MWCNT content. This suggests that the network structure of the aerogels become more robust due to the presence of MWCNTs. The porous properties of the MWCNT/PAN and MWCNT/CA aerogels are given and compared in Table 1.

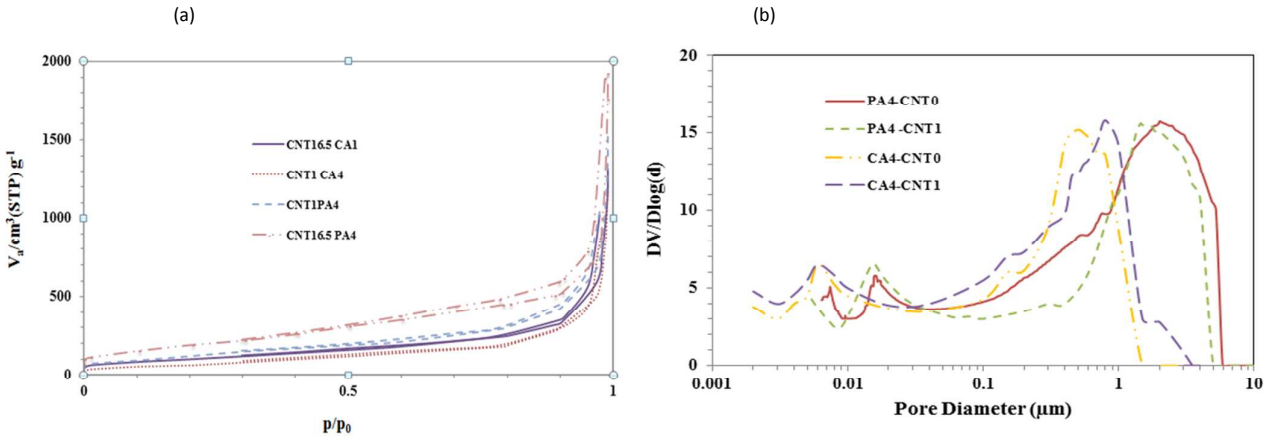

Fig. 5. (a) Nitrogen adsorption and desorption isotherms and (b) Mercury porosimetry curves of the MWCNT/PAN and MWCNT /Carbon aerogels

Table 1-The porous properties of MWCNT-PA and MWNT-CA composite

Sample code	ρ (g/cm^3) ±0.005	% $\Delta L/L$ [a] ±0.01	S_{BET} (m^2/gr) ±10	V_p [b] (cm^3/gr) ±0.01	V_v [c] (cm^3/gr) ±0.01	V_{meso} (cm^3/gr) ±0.01	V_{micro} (cm^3/gr) ±0.01	V_{total} (cm^3/gr) ±0.02	ε [d] % ±0.02	Ø [e] % ±0.01
PA4-CNT0	0.066	5.00	120	1.07	5.8	0.56	0.03	14.31	94.31	0.00
PA4-CNT0.01	0.066	4.92	173	1.24	6.01	0.71	0.09	12.76	94.41	0.01
PA4-CNT0. 1	0.065	4.87	226	1.95	6.23	0.97	0.14	15.01	94.52	0.10
PA4-CNT0.5	0.062	4.58	387	2.33	6.56	1.02	0.23	16.13	94.78	0.50
PA4-CNT1	0.060	4.35	494	2.843	7.04	1.68	0.52	16.87	95.02	1.00
PA4-CNT16.5	0.053	3.33	735	3.97	7.56	2.78	0.91	18.10	95.98	16.50
CA4-CNT0	0.540	73.68	70	0.03	0.46	0.01	0.00	1.28	69.14	0.00
CA4-CNT0.01	0.430	68.84	74	0.93	0.10	0.42	0.02	1.76	75.57	0.05
CA4-CNT0. 1	0.340	58.02	106	1.13	2.26	0.683	0.037	2.39	81.62	0. 30
CA4-CNT0.5	0.240	54.84	209	1.68	3.32	0.88	0.05	3.59	86.28	1.48
CA4-CNT 1	0.150	48.87	238	1.73	5.09	0.97	0.09	6.09	91.47	2.72
CA4-CNT 16.5	0.090	39.65	376	1.93	6.23	1.07	0.11	10.68	95.21	39.43
PA8-CNT0	0.092	1.66	43	0.74	3.12	1.01	0.00	10.58	92.25	0.00
CA8-CNT0	0.820	56.84	11	0.01	0.27	0.16	0.00	0.65	53.14	0.00
MWCNT-COOH	2.100	-	233	-		-	-	-	-	-

[a] The linear shrinkage

[b] V_p was obtained from the adsorbed N_2 volume at $P/P_0 = 0.99$. Due to the high volume of macro pores in all samples, V_p is much less than the V_{total} , which was calculated via Eq. 1

[c] total pore volume that was obtained from mercury porosimetry .

[d] porosity percent estimated from Eq.2.

[e] Volume fraction of CNT in final composites.

Journal Name

ARTICLE

The obtained data indicated that the pore size and the linear shrinkage dramatically decreased with the PAN concentration. Assuming a cylindrical pore, capillary pressure P_{cap} is given by Eq. 3: [37]

$$P_{cap} = 2\gamma_{lv}cos\theta/r_p \quad (3)$$

Where, γ_{lv} is liquid–vapor interfacial tension, θ is liquid surface contact angle and r_p is the pore radius. The ultimate shrinkage of the sample after drying is the result of a counterbalance between capillary pressures and compression strength of the sample structure. The higher capillary pressures and lower strength of the network would result in more shrinkage or even collapse of the gel during drying. Therefore, from the obtained results it can be concluded that at higher the PAN concentration , mechanical strength of the samples was large enough to overcome increased capillary forces. Also, it can be seen that for porous materials, a power law relation between strength and density exists: [38]

$$\sigma = c\rho^n \quad (4)$$

Where σ is compression strength, ρ is the bulk density, c is a constant (pre- factor), and n is a non-integer exponent that usually ranges from 2-4. So by increasing the solid content, strength of the aerogels is increased resulting in decreasing their shrinkage. The Pore volume and the BET surface area of the foams were observed to decrease during carbonization process. This may have been due to annealing of micro and meso porosity in the polymer solution in the struts of the carbon foams during the pyrolysis. Similar results have been reported by Sylvester et al. [34], in preparation of microcellular carbon foams by the high-temperature carbonization of polyacrylonitrile (PAN) foams in an inert atmosphere.

As BET surface area is mainly due to micropores and small mesopores, it decreases with decreasing micropore volume. The obtained data also indicate that the bulk density decreased and the pore volume and the S_{BET} values increased gradually with the MWCNT content. The density showed about 20% decrease for the sample containing 16.5 v% CNT. It can be attributed to the formation of a three-dimensional network of nanotubes at CNT loading of 16.5 v%, which improves the mechanical properties of composites.

The effect of MWCNT concentration on shrinkage and Monolith density of the dried and pyrolyzed samples is illustrated in Fig.6 . The results showed that the shrinkage values decreased gradually With the MWCNT content of the aerogel for the dried samples. The same trend is observed for the pyrolyzed composites process with a greater slope. These observations indicated that the MWCNT appear to reinforce the PAN aerogels framework and therefore limit the volumetric changes that occur during drying of these materials. The obtained results also showed that embedding of MWCNTs into PAN matrix can enhance the porosity of the resulting composite aerogels. This is contrary to Chen et al [22] report. They pointed out that as the MWCNT increased in formulations, both micropores and small mesopores were blocked, hence S_{BET} of as-prepared CNT aerogel reduced considerably. The obvious enhancement in porosity in our PAN/MWCNTs aerogels ascribes to uniform dispersion of MWCNTs in aerogel matrix and since PAN gel is mainly macropore, pore blockage has not occurred. Since, CNTs have a high specific surface (233 m^2/g), adding them to the PAN, can cause a significant increase in the surface area of obtained aerogel. The experimental results obtained for S_{BET} of the composite samples exceed 450 m^2/gr. However, the rule of mixtures at 1 v% CNT predicts a value of 121 for S_{BET}, The fragmentation and shortening of nanotubes after sonication combined with the increased surface roughness of PAN coated CNTs can cause observed extraordinary increase in S_{BET} of the aerogel composites.

(a) (b)

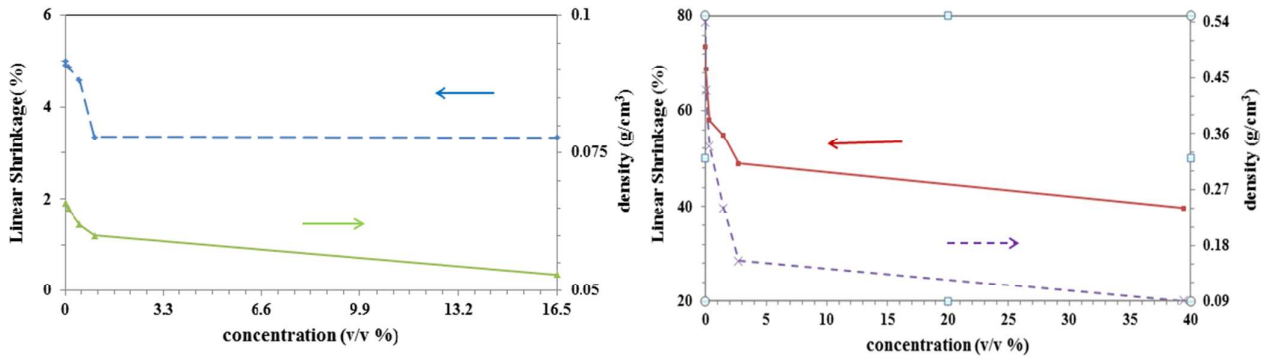

Fig. 6. Monolith density and linear shrinkage of aerogels as a function of MWCNT concentration for (a) drying and (b) pyrolysis process.

Thermal stability of carbon and polymer aerogels was investigated by TGA as shown in Fig. 7. For PAN aerogel, the first mass loss begins around 300 ˚C and is associated with nitrile oligomerization, which produces volatile products, e.g. NH_3, HCN, CH_3CN etc.[39] The second stage of the PAN degradation occurs at 350–550˚C and is related to the thermal degradation reaction of the polymer. The obtained results indicated that the rate of thermal decomposition of PAN in all MWCNT aerogels decreased with increasing MWCNT concentration. It is likely that the thermal stability of the MWCNT aerogels is increased by the incorporation of MWCNT Thus, the shrinkage of pyrolyzed samples decreased with increasing nanotube content.

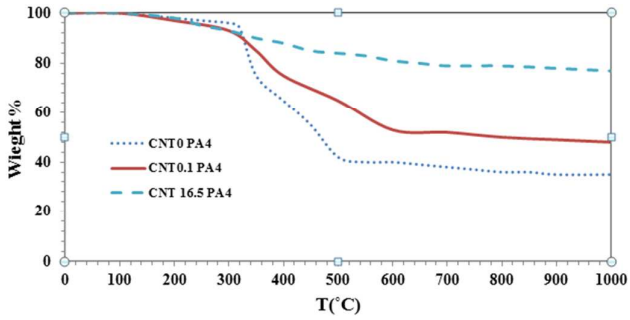

Fig. 7. TGA curves of the resulting MWCNT-PAN aerogels.

To determine the effect of the incorporation of MWCNTs into the CA matrix on the electrical properties of these materials, the relative electrical conductivity of the MWNT/CA aerogels were measured using two probe technique.

Fig. 8 shows a semi–log plot of the electrical conductivity of the MWNT/CA aerogel as a function of MWCNT concentration.

σ_{eff} and σ_m were defined as the electrical conductivity of the MWNT/CA and the pristine CA, respectively. The enhancement in electrical conductivity was chosen over absolute electrical conductivity so that MWNT/CA samples with different densities could be directly compared. The relative electrical conductivity increased slightly with MWCNT loading . The largest improvements in electrical conductivity were observed in MWNT/CAs with about 0.165 v/v MWCNTs, showing a tenfold increase in electrical conductivity. Since the electrical conductivity of MWCNT/CAs composites undergoes a continuous change with the increasing amount of nanotubes. The percolation effect can be neglected. The observation is likely due to the relatively small contrast in the electrical conductivity between CNTs and CAs as compared to the difference in conductivity between CNTs and other composite matrices, such as organic polymers.[40,41]

It seems that the obtained results are compatible with effective medium theory (EMT). This theory also enables estimation of the interfacial resistance R_σ at the MWNT/matrix interface. R_σ is characterized by a surface potential discontinuity at the MWNT/CAs interface, and reads:[42]

$$R_\sigma = \frac{\Delta V}{J} \qquad (5)$$

Where ΔV is the voltage drop and J is the applied electrical flux(current density)across the interface. The effective electrical conductivity of a composite consisting of a system of randomly oriented rods in a host medium is :[39]

$$\sigma_{eff} = \sigma_m \frac{3+\Phi(\beta_\parallel+\beta_\perp)}{3-\Phi\beta_\perp} \qquad (6)$$

Where:

$$\beta_\perp = \frac{2(d(\sigma_{CNT}-\sigma_{CA})-2R_\sigma\sigma_{CNT}\sigma_{CA})}{d(\sigma_{CNT}+\sigma_{CA})+2R_\sigma\sigma_{CNT}\sigma_{CA}} \qquad (7)$$

$$\beta_\parallel = \frac{L(\sigma_{CNT}-\sigma_{CA})-2R_\sigma\sigma_{CNT}\sigma_{CA}}{L\sigma_{CA}+2R_\sigma\sigma_{CNT}\sigma_{CA}} \qquad (8)$$

σ_{CA} and σ_{CNT} are the electrical conductivities of the CA and COOH-MWCNT respectively. For σ_{CA}, the electrical conductivity data for the pristine CA material prepared in this study were used, while a value of 10^4 S/ m (reported by the manufacturer) was used for σ_{CNT} . From TEM micrographs the MWCNTs were dispersed as bundles with diameter (d) of 15 nm and length (L) of 1000 nm. The interfacial resistance, R_σ, was used as the fitting parameter. The results showed that the effective medium theory is in good agreement with the experimental data. The value of R_σ obtained from this data was 1.26×10^{-11} Ω m^2 whose value is in agreement with data reported for similar carbon nanotube composites in other works .[28,32] In this method, the deviation of the data from the fitted curve at high MWCNT concentrations is correlated with the volume fraction of aggregated carbon nanotubes. The values calculated for different MWCNT loadings are listed in Table 3. The results showed that with the increase MWCNT volume fraction in composite, their agglomeration was increased which is in agreement with previous findings .[43]

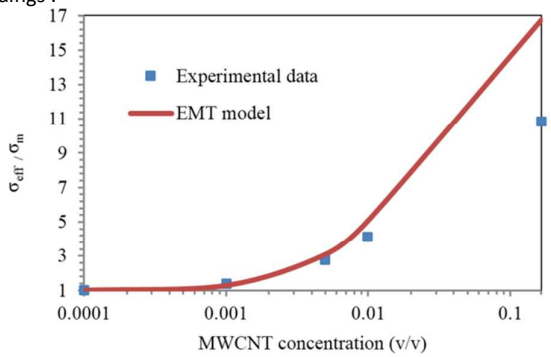

Fig. 8. Semi-log plot of relative electrical conductivity of the composites with respect to MWCNT volume fraction: experimental data (■) and EMT fit (–).

Table 2-Estimation of the amount of separated MWCNTs in MWCNT/PAN composite aerogels.

Ø	$Ø_s$ [a]	$Ø_s/Ø$ ×100 ±2
0.0001	0.000098	98
0.001	0.00098	98
0.005	0.0047	94
0.01	0.0083	83
0.165	0.0275	16

[a] the volume fraction of separated carbon nanotubes

Conclusions

This paper describes the fabrication and characterization of MWCNT/carbon aerogels using PAN as crosslink agent. These nanocomposites were synthesized for the first time by thermally induced phase separation (TIPS) of Polyacrylonitrile in MWCNT/DMF suspension. The obtained data indicated that the pore size and the linear shrinkage dramatically decreased with the PAN concentration. This was attributed to the high mechanical strength of the samples in comparison to the capillary forces. The experimental results also showed that embedding of MWCNTs into PAN matrix can enormously enhance the S_{BET} the resulting composite aerogels. The fragmentation and shortening of nanotubes after sonication combined with the increased surface roughness of PAN-coated CNTs can cause a significant increase in S_{BET} of the aerogel composites. The MWCNT/CA composites exhibit enhanced electrical conductivities relative to their respective pristine CAs. The presence of CNT aggregates led to a deviation of the electrical conductivity of the nanocomposites from the expected values calculated by EMT. These promising properties such as high porosity, surface area and electrical conductivity make MWCNT/CA nanocomposites excellent candidates for energy storage applications. Other potential applications of these MWCNT composite aerogels include catalyst supports and novel electrodes.

Acknowledgements

This work was sponsored by Space transportation research institute, Iranian research Center, Department of Nanotechnology & Nanoscience (P.O.Box 13445-754) and Institute of Nano Science and Nano Technology, Kashan University. We would like to thank Research Laboratory of Inorganic Chemistry of Tehran University for their great help in measurement of surface properties.

References

1 A. Du , B. Zhou , Z. Zhang and J. Shen , *Materials*,2013, **6** 941.
2 C. Liang, Z. Li, S. Dai, *Angew. Chem. Int. Ed*., 2008, **47**, 3696.
3 M.B. Bryning, D.E. Milkie, M.F. Islam, L.A. Hough, J.M. Kikkawa and A.G. Yodh, *Adv.Mater,*2007, **19,**661.
4 N. Job, A .Thery, R. Pirard, J Marien, L. Kocon and J.N. Rouzaud, *Carbon* ,2005 , **43**,1808-1811.
5 S.M Jung, H. Y Jung, M.S. Dresselhaus, Y. J. Jung and J .Kong, *Cientific reports*, 2012,**2**, 849.
6 M. Antonietti, N. Fechler and T. P Fellinger, *Chem. Mater*,2014, **26**,196.
7 J. H. Aubert and A. P. Sylwester, *Materials Science* ,1991, **26** 5741 .
8 Q.Y. Wu, L.S.Wan and Z. K. Xu, *Membrane Science*,2012, **409** , 355.
9 Q.Y Wu, L.S Wan and Z. K Xu, *Polymer* ,2013, **54**,284 - 291.
10 H. Q Liang, Q. Y. Wu, L. S. Wan, X. J. Huang and Z. K . Xu, *Membrane Science,2014,* **465** 56.
11 M. Moniruzzaman and K. I. Winey, *Macromolecules* ,2006, **39**,5194.
12 P. M. Ajayan and J. M. Tour, Nature ,2007, 447, 1066.
13 S .Nardecchia, D. Carriazo, M. L. Ferrer, M. C. Gutierrez and F. Monte, Chem.Soc.Rev, 2013, 42, 794.
14 T .Bordjiba and M .Mohamedi, *Solid State Electrochem*, 2011,**15**, 765.
15 G. Lalwani, A. T. Kwaczala, S .Kanakia, S. C. Patel, S . Judex and B. Sitharaman, *Carbon* ,2013, **53**, 90.
16 M. B. Bryning , D. E. Milkie , M. F. Islam , L. A. Hough , J. M. Kikkawa and A. G. Yodh , *Adv. Mater*, 2007 , **19** , 661.
17 K. H. Kim , M. Vural and M. F. Islam , *Adv. Mater,* 2011 , **23** 2865.
18 K.H. Kimand M. F. Islam, *Nat. Nanotechnol* , 2012,**7**,562.
19 S.N. Schiffres, K.H. Kim, L Hu, M.F.Islam and J.A. Malen, *Adv. Funct. Mater*, 2012, **22**,5251.
20 L. A. Hough , M. F. Islam , B. Hammouda , A. G. Yodh and P. A. Heiney , *Nano Lett,* 2006,**6**, 313 .
21 J .Chen, C. Xue , R .Ramasubramaniam and H .Liu, *Carbon* , ,2006,**44**, 2142.
22 R. Kohlmeyer, M .Lora, J .Deng, H. Liu and J .Chen, *Carbon*,2011, **49** ,2352.
23 X. Zhang, D. Chang, J. Liu and Y. Luo, *Mater Chem* ,2010,**20**,5080.
24 X. Zhang , J. Liu ,B. Xu, Y. Su and Y. Luo, *Carbon*, 2011, **49** 1884.
25 I .Zou, J. Liu, A.S Karakoti, A. Kumar, D. Joung, Q . Li, S. I. Khondaker, S, Seal and L. Zhai, *ACS Nano* ,2010,**4**, 7293.
26 M. A. Worsley, J. H. Satcher and T. F. Baumann, *Langmuir*, 2008,**24**,9763.
27 M. A. Worsley, J. H. Satcher, and T. F. Baumann , *Appl Phys Lett* , 2009,**24**,073115.
28 M. A. Worsley, P.J. Pauzauskie, S.O. Kucheyev, J.M. Zaug, A.V. Hamza, *Acta Mater* , 2009,**57**, 5131–5136.
29 M. A. Worsley, S.O. Kucheyev, J.D. Kuntz, A.V. Hamza and J.H. Satcher, *Mater. Chem,* 2009,**19**,3370.
30 J. Shin , S. O. Kucheyev, M. A. Worsley and A. V. Hamza, *Carbon* ,2012, **50**, 5340.
31 M . Haghgoo, A.A Yousefi, M. J. Zohouriaan Mehr, A .Celzard, V. Fierro, A. Léonard and N .Job , *Microporous and Mesoporous Materials* , 2014,**18**,497.
32 M .Haghgoo, E .Plougonven, A.A.Yousefi, J. P. Pirard, A. Léonard, N. Job, *Carbon* ,2012,**50**,1447.
33 E. Fitzer, W. Frohs and M. Heine, *Carbon* ,1986,**24** , 387.
34 J. H. Aubert, A. P. Sylwester, Materials Science ,1991, 26,5741.
35 M .Wiener, G .Reichenauer, T .Scherb and J .Fricke , *Non-Cryst Solids* ,2004,**350**, 126.
36 Y.Cui and M.Zhang, *ACS Appl. Mater. Interfaces,* 2013, **5 (16)**, 8173.
37 T. Heinrich, U .Klett and J. Fricke , *Porous Mat* ,1995,**17**,1.
38 R.W.Pekala, C.T. Alviso and J. D. LeMay, *Non-Crystalline Solids*, 1990, **125**,67-75.
39 A. V. Korobeinyk, R.L.D. Whitby and S. V. Mikhalovsky, *European Polymer* ,2012, **48** ,97.
40 M.B. Bryning, Carbon Nanotube Networks in Epoxy Composites and Aerogels, Ph.D. Thesis, University of Pennsylvania, 2007.
41 L.Gao, X.Zhou and Y. Ding, Chemical Physics Letters, 2007, **434**, 297.
42 D. Richard, M. Fafard, R. Lacroix, P. Cle´ry and Y. Maltais, *Materials Processing Technology* ,2003, **132** ,119.
43 X.L. Xiea, Y.W. Maia, X. P. Zhou, *Materials Science and Engineering: R: Reports* , 2005, **49** ,89.